Eur. Phys. J. A **36**, 359–364 (2008)
DOI 10.1140/epja/i2008-10598-1

THE EUROPEAN PHYSICAL JOURNAL A

Regular Article – Theoretical Physics

Deuterium-deuterium nuclear cross-sections in insulator and metallic environments

D. Salzmann[1] and M. Hass[2,a]

[1] Marganit 2, Ness Ziona 74051, Israel
[2] Department of Particle Physics, Weizmann Institute of Science, Rehovot, Israel

Received: 7 April 2008
Published online: 17 June 2008 – © Società Italiana di Fisica / Springer-Verlag 2008
Communicated by G. Orlandini

Abstract. The three-dimensional Thomas-Fermi (TF) model is used to simulate the variation of the $d+d \rightarrow t+p$ cross-section at low impact energies, when the target deuterium nucleus is embedded in metallic or insulator environments. The comparison of the computational results to recent experiments demonstrates that even though the TF model can explain some increase in the low-energy cross-section for metallic host, a full explanation of the experimental results is still lacking. Possible reasons for the disagreement are discussed.

PACS. 95.30.-k Fundamental aspects of astrophysics – 95.30.Dr Atomic processes and interactions

1 Introduction

In a series of recent experiments [1–6] significant differences had been found between the low-energy cross-sections of the $d + d \rightarrow t + p$ reaction when the target nuclei are embedded in a metallic or an insulator environment. Apparently, the source of this effect is the conduction electron distribution in the metallic lattice and its screening effects on the Coulomb barrier around the incident and target nuclei [7,8]. Hints for a similar behavior were found also in the electron capture rate of Be^7 [9, 10]. While in some of these experiments temperature dependence was also claimed [1,2], no such dependence was found in others [9,11].

This phenomenon can be briefly introduced as follows: The transparency, $T(E_k)$, of a potential barrier to an incident particle having energy E_k is given by [12]

$$T(E_k) = \exp\left\{-2\int_{r_N}^{b}\sqrt{\frac{2M}{\hbar^2}[E_p(r) - E_k]}\mathrm{d}r\right\}, \qquad (1)$$

where M is the reduced mass of the two particles, r_N the nuclear radius, b the classical turning point (CTP) and $E_p(r) = ze\,V(r)$ is the potential energy of the incident particle in the potential, $V(r)$, generated by the target nucleus. Ze and ze are the charges of the target and incident nuclei, respectively.

[a] e-mail: michael.hass@weizmann.ac.il

If a pure Coulomb potential is substituted for the interaction potential, $V(r) = V_{\mathrm{C}}(r) = Ze/r$, eq. (1) reproduces the Sommerfeld factor

$$T_{\mathrm{C}}(E_k) = \exp\left\{-2\int_{r_N}^{b}\sqrt{\frac{2M}{\hbar^2}\left[\frac{Zze^2}{r} - E_k\right]}\mathrm{d}r\right\}$$
$$= \exp\{-2\pi\eta\}, \qquad (2)$$

$$\eta(E_k) = \frac{Zz\,e^2}{\hbar v_k}. \qquad (3)$$

In (3) $v_k = \sqrt{2E_k/M}$ is the velocity of the incident particle. If the target nucleus is embedded in a solid target, the potential generated by nearby electrons, in addition to the bare Coulomb potential, has to be included as well,

$$V(r) = V_n(r) + V_e(r) = \frac{Ze}{r} + V_e(r). \qquad (4)$$

For low-energy reactions the electronic part of the potential, $V_e(r)$, has a small but important contribution to the total potential. This contribution is amplified by the exponential factor of the transparency.

In general, the electronic potential generated in a metallic lattice by the conduction electrons is a slowly varying function. Even for low-energy particles the CTP of the projectile is so close to the target nucleus that one can fairly assume that along the integration path in (1) the electronic potential practically equals its value at the target nucleus, $V_e(r) \cong V_e(0)$. When this approximation

is inserted back into (1) it gets the form,

$$T(E_k) \cong \exp\left\{-2\int_{r_N}^{b}\sqrt{\frac{2M}{\hbar^2}\left[\frac{Z z\, e^2}{r}+zeV_e(0)-E_k\right]}\,\mathrm{d}r\right\}. \tag{5}$$

This is equivalent to a reaction in a pure Coulomb potential with the kinetic energy, E_k, replaced by E_k+U_e, where

$$U_e = ze\,|V_e(0)|, \qquad (V_e(0)<0). \tag{6}$$

The authors of ref. [1] tried to explain the experimental results by means of the Debye statistical model, which neglects the electrons degeneracy. A difficulty of their treatment is also the point that under the stated experimental conditions the Debye radius is significantly smaller than the atomic radius, therefore the basic assumptions of the model are not satisfied.

The aim of the present paper is to compute the electrons spatial distribution in insulator and metallic environments for the $d+d \rightarrow t+p$ reaction ($Z=z=1$), using a three-dimensional Thomas-Fermi (TF) model, which accounts for the electrons' degeneracy, therefore, presumably better describing the experimental conditions in a solid host of local high-density conditions ("strongly-coupled plasma"). Using the TF model we try to infer the change in the transparency between metallic and insulating environments. To illustrate our method, we shall focus on the case of deuterium embedded in a copper lattice for which experimental results are available [1].

2 The model

2.1 Basic data

In the experiment, ref. [1], the deuterium atom constitutes only a small part of the target —about 11 copper atoms for each deuterium atom [1]— one can, therefore, safely assume that the presence of the deuterium atoms does not significantly modify the copper lattice properties.

Our first step is to find the volume available for the deuterium atoms. This is carried out by means of the QEOS method [13], which is frequently used to find the equation of state of various materials, and was found to give accurate results. For our purposes its main advantage is that QEOS can provide the volume per atom separately for each component in a mixture of materials. Assuming a deuterium/copper solid material with 9% deuterium and 91% copper at $8.93\,\mathrm{g/cm^3}$ (solid copper specific gravity), QEOS predicts that the volumes of the deuterium (copper) atoms in the target are $\mathrm{Vol_D}\,(\mathrm{Vol_{Cu}}) = 1.79\,(11.7)\cdot 10^{-24}\,\mathrm{cm^3/atom}$, *i.e.*, the average volume available for a copper atom is by a factor of ~ 6.5 larger than that of a deuterium atom. If these atomic volumes are assumed to have the shape of a spherical enclosure, called in the following the *ion sphere* (IS), then the corresponding IS radii are $R_{i,\mathrm{D}}\,(R_{i,\mathrm{Cu}}) = 0.717\,(1.36)\,10^{-8}\,\mathrm{cm}$.

The atomic structure of copper is $[Ar]\,3d^{10}\,4s$. In a pure copper metal lattice there are at most 11 electrons per atom in the conduction band. Their average density is $n_e = 11/11.7\cdot 10^{-24} = 9.4\cdot 10^{23}$ electrons/cm^3. If the small amount of deuterium atoms does not significantly change this distribution, then the same density prevails within the deuterium IS as well, generating $n_e \mathrm{Vol_D} = 9.4\cdot 10^{23}\times 1.79\cdot 10^{-24} = 1.7$ extra electrons inside the deuterium IS. Thus, together with its own electron, the deuterium IS contains, on the average, $N_e = 2.7$ electrons. Changing the Cu/D target density by $\pm 10\%$ changes this quantity only by $\pm 5\%$. In our computations we have used N_e, the number of electrons in the deuterium IS, as an adjustable parameter.

2.2 The modelling of the electronic potential in insulating and metallic environments

The electronic potential of a free deuterium atom in a high-density insulating environment was calculated by the computer program RELDIR, which solves the relativistic Dirac equation of a deuterium (or any other) atom in a finite radius ion sphere with any number of free electrons within the IS. The results of this computation are the bound and free electrons wave functions, their spatial density, and the corresponding potentials.

As a first step, the computation was carried out for a solid density deuterium lattice, which is known to be an insulator, ($0.202\,\mathrm{g/cm^3}$, $6.08\cdot 10^{22}$ atoms/cm^3, $R_i = 1.58\cdot 10^{-8}\,\mathrm{cm}$). From the result of RELDIR for the electronic potential one obtains $U_e = 20\,\mathrm{eV}$, in accordance with the experimental results of ref. [1] in an insulating environment. This result was used as the basic reference for comparison.

The evaluation of the electronic potential near a deuterium atom embedded in a metallic lattice was carried out by means of the Thomas-Fermi (TF) model in conjunction with the Born-Oppenheimer (BO) approximation. Owing to the high-density environment, a Fermi-Dirac statistics for the electrons, as used by the TF model, provides a better approximation for the electrons spatial and energy distributions inside the copper lattice than the Debye model [1,2] which is more appropriate for weakly coupled low-density matter. In this context, the physical meaning of the BO approximation is that nearby electrons rapidly adjust their local distribution to any change in the nuclei positions, so that the electron distribution depends only on the instantaneous distance between the two nuclei, but not on their relative motion.

The TF model for the electrons consists of a set of three equations. The first one is the Poisson equation,

$$\boldsymbol{\nabla} V_e(\mathbf{r}) = 4\pi e\, n_e(\varepsilon_\mathrm{F};\mathbf{r}), \tag{7}$$

whose solution is the electronic potential, $V_e(\mathbf{r})$, when the electrons spatial density, $n_e(\varepsilon_\mathrm{F};\mathbf{r})$, is known. In (7) ε_F is the Fermi energy. The second equation is the Fermi-Dirac distribution of the electrons inside the IS,

$$n_e(\varepsilon_\mathrm{F};\mathbf{r}) = \frac{1}{2\pi^2}\left(\frac{2m_e\,kT}{\hbar^2}\right)^{3/2} \times F_{1/2}\left(\frac{\varepsilon_\mathrm{F}+eV(\mathbf{r})}{kT};\left|\frac{eV(\mathbf{r})}{kT}\right|\right), \tag{8}$$

which provides the electron density as a function of the total potential $V(\mathbf{r}) = V_n(\mathbf{r}) + V_e(\mathbf{r})$. In (8), kT is the temperature of the target material (= 300 K) in energy units, and

$$F_{1/2}(x;\beta) = \int_\beta^\infty \frac{y^{1/2}\,\mathrm{d}y}{1+\exp\{y-x\}} \tag{9}$$

is the *incomplete Fermi-Dirac integral* [14]. The boundary condition applied to eqs. (7) and (8) is Gauss' theorem, $\oint_{\text{IS surface}} \mathbf{E}\cdot\mathrm{d}\mathbf{S} = 4\pi e\,N_e$. Finally, the Fermi energy, ε_F, is computed from the condition that the total charge inside the IS equals N_e,

$$N_e = \int_{\text{IS volume}} n_e(\varepsilon_\mathrm{F};\mathbf{r})\,\mathrm{d}^3r. \tag{10}$$

The simultaneous solution of eqs. (8)–(10) yields the electronic potential, $V_e(\mathbf{r})$, the electron density, $n_e(\varepsilon_\mathrm{F};\mathbf{r})$, and the Fermi energy, ε_F. When these solutions are inserted back into (1) and (4), one finds the CTP, $b(N_e, E_k)$, and the transparency, $T(N_e, E_k)$ as a function of the number of electrons inside the IS and the incident particle's kinetic energy.

2.3 Computational details

The solution of (7) can be rewritten as [15],

$$\begin{aligned} V_e(r,\theta,\varphi) &= -e\iiint_{\text{IS volume}} \frac{n_e(r',\theta')}{|\mathbf{r}-\mathbf{r}'|}\mathrm{d}^3r \\ &= -e\int_{r_N}^{R_i} r'^2\,\mathrm{d}r' \int_{\theta=0}^{\pi} \sin\theta'\,\mathrm{d}\theta' \\ &\quad\times\int_{\varphi=0}^{2\pi}\mathrm{d}\varphi'\,\frac{n_e(r',\theta')}{|\mathbf{r}-\mathbf{r}'|}\,. \end{aligned} \tag{11}$$

Obviously, the electron distribution has cylindrical symmetry around the line connecting the two nuclei, therefore $n_e(r',\theta')$ is independent of φ'. Moreover, the charge distribution has also a reflection symmetry around the plane perpendicular to this line at halfway between the nuclei. Using these symmetry properties, the integration over φ' can be carried out analytically, thereby reducing the triple integral in (11) to a double one, see details in ref. [15]. Finally, transforming the coordinate system center onto the target nucleus, eq. (11) gets the form,

$$\begin{aligned} V_e(R,\mu) &= -4e\int_{r_N}^{R_i} R'^2\,\mathrm{d}R' \int_{\mu=\mu_{\min}}^{1} \mathrm{d}\mu'\,n_e(R',\mu') \\ &\times\left[\frac{1}{\sqrt{A_-+B}}K\left(\sqrt{\frac{2B}{A_-+B}}\right)+\frac{1}{\sqrt{A_++B}}K\left(\sqrt{\frac{2B}{A_++B}}\right)\right], \end{aligned} \tag{12}$$

$$\begin{aligned} A_\pm &= \left[(b/2+R\cos\theta)\pm(b/2+R'\cos\theta')\right]^2 \\ &\quad +(R\sin\theta)^2+(R'\sin\theta')^2\,, \end{aligned} \tag{13}$$

$$B = 2R\,R'\,\sin\theta\,\sin\theta'\,. \tag{14}$$

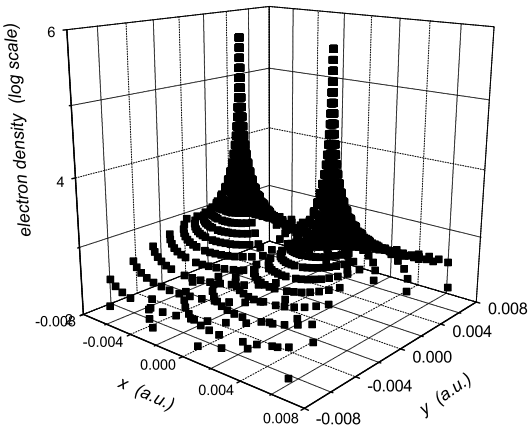

Fig. 1. The distribution of the electrons around the two nuclei.

In (12) R is the radial distance of the field point from the target nucleus, $\mu = \cos\theta$, $K(x)$ is the Jacobi elliptic integral [16], and $\mu_{\min} = \max(-b/2R', -1)$. The reduction of the triple integral in (11) to the shape of (12) reduced the computational resources and improved the accuracy of the numerical procedure.

The numerical process was greatly complicated by the fact that the CTP, b, not only depends on the electron density, $n_e(\varepsilon_\mathrm{F};\mathbf{r})$, but also determines it. It was, therefore, necessary to carry out a doubly iterative method for the computations. The internal iterations calculated the electron density and potential through eqs. (12)–(14) and (8)–(10). When these have been found, a second iterative procedure was applied to solve b from the condition,

$$E_p(b) = E_k\,. \tag{15}$$

This doubly iterative method was continued until convergence was achieved for all the parameters.

3 Results

3.1 The electron density

Figure 1 shows the density of the electrons around the incident and the target nuclei, when the center-of-mass energy of the two nuclei is 4000 eV. The figure clearly shows the polarization of the electrons near the nuclei. We recall that the TF model predicts that the electron density diverges as $r^{-3/2}$ near the nucleus [14].

The TF model predicts an accumulation of the electrons along the line connecting the nuclei, with a saddle point at halfway between them, a fact which enhances the screening effect.

3.2 The electronic potential

Figure 2 shows the spatial distribution of the electronic potential in the same region as in fig. 1. In the interesting part of the field, *i.e.* in the space around the two nuclei,

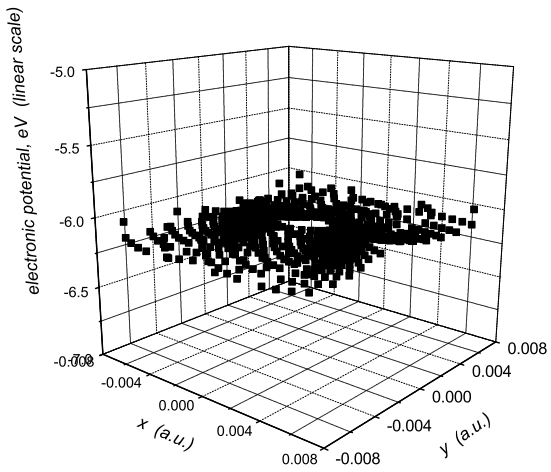

Fig. 2. The distribution of the electronic potential, $V_e(r)$, around the two nuclei.

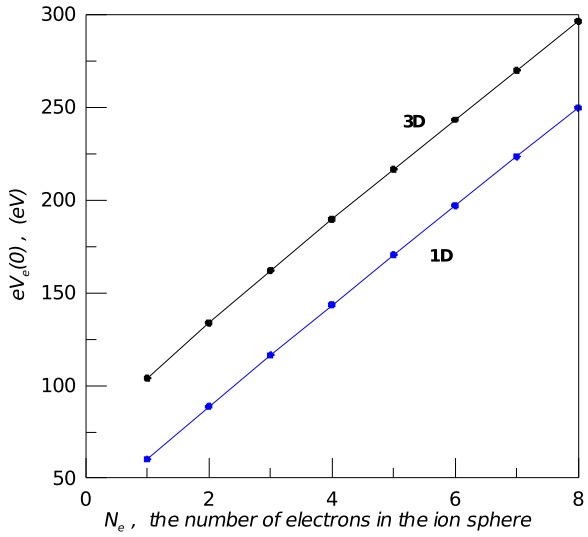

Fig. 3. The value of the electronic potential, $V_e(r)$, on the target nucleus.

the potential has very slow variation, which justifies the approximation $V_e(r) \cong V_e(0)$, to an accuracy of a few percents.

The value of the potential on the nuclei, $U_e = |eV_e(0)|$, is displayed in fig. 3. This is, in fact, the quantity that is measured experimentally. The figure shows that U_e fits excellently a linear behavior as a function of N_e, with a small contribution from the incident energy,

$$\text{3D: } U_e = |eV_e(0)| = 27.2\,N_e + 80.3 + 3.1\cdot 10^{-4} E_k \,\text{eV}. \quad (16)$$

The last term is always less than 4% in the range of interest. In order to compare the importance of a 3D modelling, we have developed also a one-dimensional TF program that solves the same problem in a radially symmetrical environment. The results of this program is also plotted in fig. 3. The TF 1D code yielded,

$$\text{1D: } U_e = |eV_e(0)| = 27.2\,N_e + 33.6\,\text{eV}. \quad (17)$$

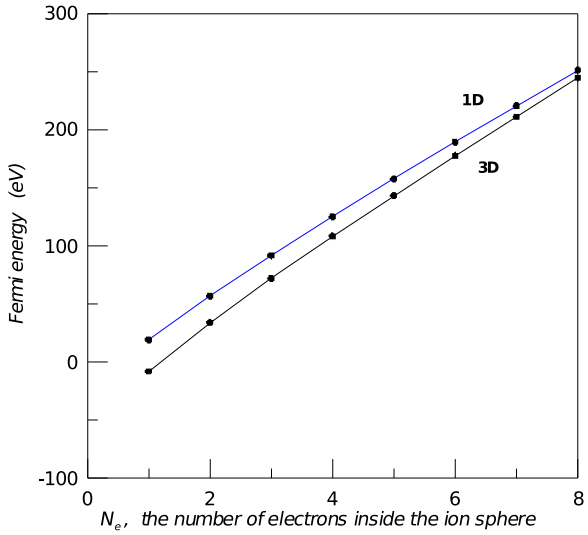

Fig. 4. Fermi energy as a function of the number of electrons inside the ion sphere, for 3D and 1D Thomas-Fermi simulations.

The difference between these two results originates from the fact that the electrons accumulation between the nuclei in a 3D model is larger than in the 1D case. This difference clearly indicates the importance of a three-dimensional treatment of the problem.

For $N_e = 3$, $E_k = 4000\,\text{eV}$, eq. (16) gives $U_e = 163\,\text{eV}$. This has to be compared to the experimental result, $U_e = 470 \pm 50\,\text{eV}$, which is by a factor of 2.9 ± 0.3 larger than the result of the TF 3D model. It has also to be compared to $U_e = 20\,\text{eV}$ as computed from RELDIR for the insulator case, see above.

3.3 The Fermi energy

The Fermi energy, ε_F, strongly depends on the number of electrons in the IS, N_e, and is, of course, independent of the incoming particle's energy. The behavior of ε_F *vs.* N_e is illustrated in fig. 4. Within the range of our computations ε_F turned out to be a linear function of N_e,

$$\text{3D: } \varepsilon_\text{F} = -43.7 + 38.8\,N_e \;(\text{eV}) \quad (18)$$

with a hint for a slight quadratic curvature. For the 1D case we have found a significantly higher result,

$$\text{1D: } \varepsilon_\text{F} = -15.9 + 35.3\,N_e \;(\text{eV}). \quad (19)$$

It should be emphasized that the Fermi energy is positive (except for the case of $N_e = 1$, namely, the case of an isolated deuterium atom), and is much higher than the target temperature ($\varepsilon_\text{F} \gg kT = 300\,\text{K} = 0.025\,\text{eV}$), for all the cases. This means that at the temperatures of the experiments (room temperature and below) there is no reason for measurable temperature variations. In fact, we have repeated our computations with $T = 3000\,\text{K}$, but this order of magnitude change in the temperature modified the results by less than 0.5%, as expected.

3.4 The classical turning point

The CTP fits, with excellent accuracy, a function of the form

$$b/a_0 = \frac{e^2/a_0}{E_k + U_e}\,, \tag{20}$$

where $e^2/a_0 = 27.211\,\mathrm{eV}$ (a_0 is the Bohr radius). This has exactly the form of the Coulomb CTP, with the projectile's kinetic energy modified according to eq. (5). Fitting the computational results to the form of (20) provides

$$U_e = 27.7\,N_e + 76.4 + 5.76\cdot 10^{-4}\,E_k\,\mathrm{eV}. \tag{21}$$

The agreement of this U_e with the values obtained from the electronic potential, eq. (16), can be regarded as very good. The difference between the two results stems from the fact that $|eV_e(\mathbf{r})|$ is not exactly constant along the line connecting the two nuclei. And again, this result is in discrepancy with the experimental value, but is much higher than the insulator case.

3.5 The transparency

At low impact energies the screened astrophysical factor, $S(E)$, is enhanced relative to the unscreened one by $T(E)/T_\mathrm{C}(E)$ [1], see eqs. (1) and (2). Figure 5 shows our results for this factor as a function of the center-of-mass energy for the $d + d \rightarrow t + p$ reaction, when the target deuterium is embedded in a copper lattice. The experimental results of ref. [1] are also displayed in fig. 5. The dashed curve represents the bare $S(E)$ factor [1]. While we note that the value $N_e = 3$ is a reasonable estimate for the conducting electrons in the deuterium IS embedded in Cu, even for $N_e = 8$ the 3-dimensional TF model underestimates the experimental low-energy increase of the astrophysical factor. The low U_e predicted by the model relative to the experiment is another manifestation of the same fact. In fact, one needs 11 conduction electrons inside the deuterium IS to get agreement with the experimental results.

In the range of the energies used in our computations $U_e \leq 0.1E$. Denoting $\xi = U_e/E$, ξ can be assumed to be a small quantity. Using first-order expansion, an analytical estimate can be developed for the change in the value of $T(E)/T_\mathrm{C}(E)$ caused by a change $b \rightarrow b/(1+\xi)$ in the CTP, see eq. (20). The ratio of the screened to Coulomb transparencies becomes,

$$T(E)/T_\mathrm{C} = \exp\{\delta G\}, \tag{22}$$

where

$$\delta G = G - G_\mathrm{C} = 2e^2\sqrt{\frac{2M}{\hbar^2}}\frac{\xi}{\sqrt{E}}\left(\frac{\pi}{4} - \sqrt{\frac{\xi}{2}}\right). \tag{23}$$

For $E = 4000\,\mathrm{eV}$, $N_e = 3$ and $U_e = 163\,\mathrm{eV}$ this formula predicts

$$T(E)/T_\mathrm{C} = \exp\{\delta G\} = 1.45, \tag{24}$$

in contrast to the experimental result of $T(E)/T_\mathrm{C} \approx 2.0 \pm 0.2$.

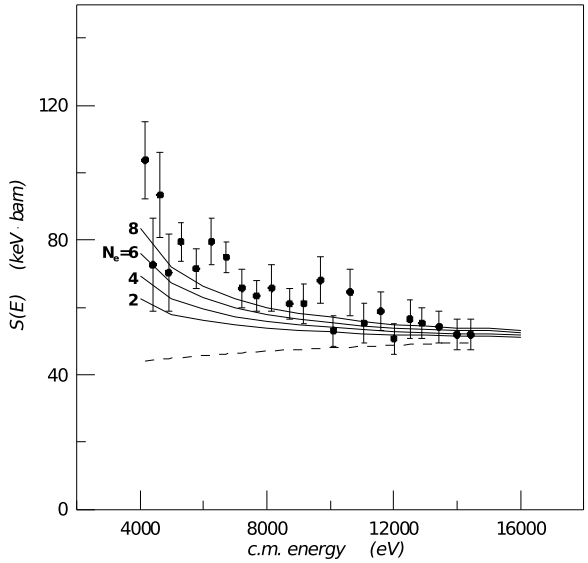

Fig. 5. Comparison between the results of the 3D TF model for the astrophysical factor, $S(E)$, of the reaction $d+d \rightarrow t+p$, when the target nuclei are embedded in a copper substrate, and the experimental results. The experimental points are taken from [1]. The dashed line presented the theoretically extrapolated "bare nucleon" $S(E)$ factor.

4 Discussion

In this paper we present computational results from a three-dimensional TF model about the modification of the low-energy cross-section for the $d + d \rightarrow t + p$ reaction, when the target nucleus is embedded in a copper lattice. Our computational result of $U_e = 163\,\mathrm{eV}$ is lower by a factor of ~ 3 from the experimental result of $U_e = 470 \pm 50\,\mathrm{eV}$, but still is substantially higher than the cross-section in an insulator (solid deuterium lattice), $U_e = 20\,\mathrm{eV}$.

In order to see whether such a difference holds true for other target lattices as well, in fig. 6 we plotted the results of all the experiments in metal lattices published in ref. [1] in comparison to ours. The 3D TF results in the figure may be shifted $\pm 5\%$ up or down, due to differences in the local IS volume of the deuterium in the various lattices. Figure 6 exhibits a consistent difference between the computational and the experimental results. As the Thomas-Fermi is a highly successful model, well fitted to high-density matter, this insistent difference is of some surprise.

Obviously, the central reason for the disagreement is the electronic potential on the target nucleus, see eq. (6). In our opinion, the semiclassical nature of the TF model cannot be the reason for this difference, because the quantum-mechanical behavior of the conduction electrons seems to be unimportant in the present problem.

On the other hand, the TF model assumption of a perfect spherical symmetry, and the target nucleus location at the center of a well-defined ion sphere, may oversimplify the real situation. In the experiment, the deuterium nuclei are implanted into the metal lattice by bombardment of 10 keV deuterons into the metal foil [2]. It is well

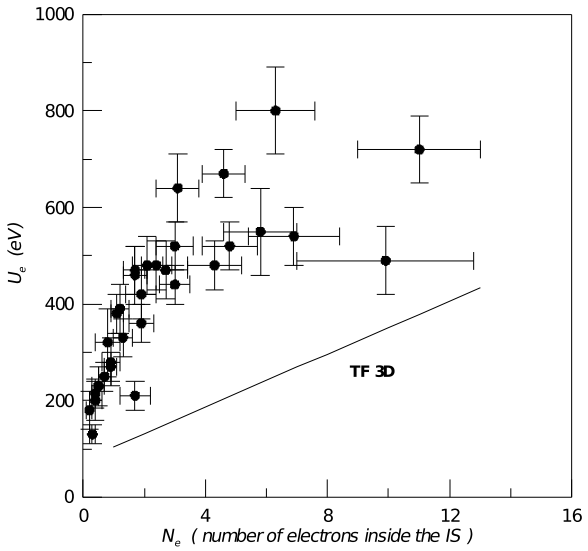

Fig. 6. The experimental values of U_e, drawn from the results of [1], compared to the predictions of the 3D TF model.

known that this technique does not necessarily deposit the stopped deuterium into a spherically symmetrical environment.

Another contribution to the discrepancy may be the local conduction electron density fluctuations around the target nucleus. As the transparency depends exponentially on the local electron potential, a small number of nuclei, with an instantaneous large electron screening, has greater influence on the cross-section than the other nuclei with the average electronic screening.

Finally, it is possible that QEOS underestimates the deuterium IS volume under the specific experimental conditions. A larger IS volume, with more conduction electrons, may have a better agreement with the experiment.

References

1. F. Raiola *et al.*, Eur. Phys. J. A **19**, 283 (2004).
2. F. Raiola *et al.*, Eur. Phys. J. A **13**, 377 (2002).
3. K. Czerski *et al.*, Europhys. Lett. **54**, 449 (2001).
4. H. Yuki *et al.*, JETP Lett. **68**, 823 (1998).
5. F. Raiola *et al.*, Phys. Lett. B **547**, 193 (2002).
6. C. Bonomo *et al.*, Nucl. Phys. A **719**, 37c (2003).
7. H.J. Assenbaum *et al.*, Rep. Prog. Phys. **50**, 233 (1987).
8. H.J. Assenbaum *et al.*, Z. Phys. A **327**, 461 (1987).
9. Y. Nir-El *et al.*, Phys. Rev. C **75**, 012801(R) (2007).
10. B. Wang *et al.*, Eur. Phys. J. A **28**, 375 (2006).
11. N. Severijns *et al.*, Phys. Rev. C **76**, 024304 (2007); V. Kumar *et al.*, Phys. Rev. C **77**, 051304(R) (2008).
12. E. Fermi, *Lecture Notes* (University of Chicago, 1949).
13. R.M. More *et al.*, Phys. Fluids **31**, 3059 (1988).
14. D. Salzmann, *Atomic Physics in Hot Plasmas* (Oxford University, New York, 1998).
15. D. Salzmann, Phys. Rev. A **49**, 3729 (1994).
16. M. Abramowitz, I.A. Stegun, *Handbook of Mathematical Functions* (Dover, New York, 1972).